Measurement 149 (2020) 106948

Contents lists available at ScienceDirect

Measurement

journal homepage: www.elsevier.com/locate/measurement

High-resolution angular measurement arithmetic based on pixel interpolations

Hai Yu [a,*], Xingdan Jia [a,b], Qiuhua Wan [a], Changhai Zhao [a], Ying Sun [a]

[a] Changchun Institute of Optics, Fine Mechanics and Physics, Chinese Academy of Sciences, Changchun 130033, People's Republic of China
[b] Graduate University of Chinese Academy of Sciences, Beijing 100039, People's Republic of China

ARTICLE INFO

Article history:
Received 19 November 2018
Received in revised form 8 August 2019
Accepted 10 August 2019
Available online 23 August 2019

Keywords:
Angular measurement
Pixel Interpolations
High-resolution
Image sensor

ABSTRACT

Image angular displacement measurement devices are equipped with image sensors which identify calibration grating to digitalize angular displacement outputs. It is easier to realize high-resolution angular displacement measurement than the traditional optical moiré fringe measurement method in a miniaturized device. This paper proposes a high-resolution angular displacement measurement algorithm based on pixel interpolation which was designed to resolve the measurement output error caused by low pixel resolution in the image sensor. An optical path for angular displacement measurement using a linear image sensor close to the calibration grating is proposed. We find that the effects of insufficient pixel quantity in the range of the grating marking line can be ameliorated using a high-resolution measurement algorithm based on pixel interpolation. The proposed algorithm is applied to simulated and experimental image angular displacement measurements to verify its performance. The results show that the proposed algorithm markedly improves the measurement resolution when the number of pixels in the range of marking lines detected by the image sensor is insufficient. We achieve a resolution of 0.15″ and accuracy of 12.93″ with circular grating diameter of 38 mm. The results presented here may enhance the theoretical basis of high-resolution angular displacement measurement.

1. Introduction

Photoelectric angular displacement measurement technology serves to convert photoelectric displacement signals into digital angular displacement signals for the purposes of industrial, aerospace, military, and other applications. It has high resolution and high precision and is easy to miniaturize, among other advantages. Advancements in science and technology have brought about increasingly stringent requirements for such technology, which has made miniaturized, high-resolution angular displacement measurement technology a popular research topic.

In the traditional measurement method, calibration grating is used to draw a moiré figure from which the photo electricity signal is collected by photoelectric conversion (Fig. 1) [1–7].

The traditional method does not readily yield high precision measurements when the grating is small. The measurements are influenced by the diversity among elements, the installation of the grating, the strength of the light source, and the range and phase of the moiré figure [8]. Noise and A/D conversions also may impact the measurement resolution. Using an image detector to measure angle displacement tends to work better in developing digital images and applying imagery principles [9–15].

Researchers in the United States [16,17], Japan [18], Spain [19], Korea [20], China [21–22] and other countries have made notable advancements in image type encoding, but the resolution of existing methods is relatively low. There has also been relatively little research on grating angular measurement, and existing array image detectors have low frequency response.

In our previous research, we used an imaging lens to obtain grating images; this setup functions properly but the device volume cannot be further reduced [23–24]. To achieve high-resolution angular displacement measurement in a smaller volume, we designed a linear image sensor which fits snugly against the calibration grating. In this setup, a circular grating projection image is acquired, processed via the appropriate algorithm, then used to realize the high-resolution measurement of the current grating angular displacement. When the resolution of the image sensor is low, the number of pixels in the pattern of the grating marking line is insufficient; this produces errors in the angular displacement measurement data obtained by calculation and renders the device altogether unreliable. We propose a high-resolution angular displacement measurement algorithm based on pixel interpolation to resolve this problem. The algorithm inserts

* Corresponding author.
E-mail addresses: yuhai5158@163.com, yuhai@ciomp.ac.cn (H. Yu).

https://doi.org/10.1016/j.measurement.2019.106948
0263-2241/

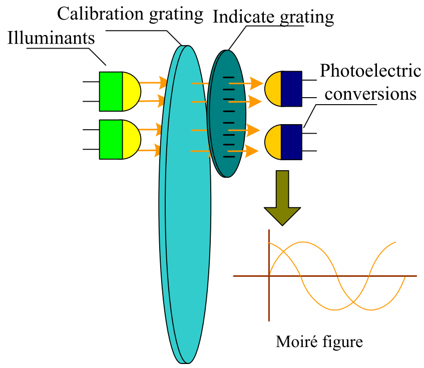

Fig. 1. Traditional measurement method.

estimated pixel points between the pixels of the collected images, then reveals a new set of pixels which can be computed through angular displacement to obtain accurate displacement information.

The rest of this paper is organized as follows. Section 2 introduces the principle of small-size angular displacement measurement using linear image sensors. Section 3 proposes the angular displacement algorithm based on pixel interpolation. Section 4 reports our simulation results and Section 5 our experimental verification. Section 6 is a brief summary and conclusion.

2. Principle of image angular displacement measurement

We used a linear image sensor to obtain a calibration grating pattern to improve the angular displacement measurement frequency response. This principle is illustrated in Fig. 2.

In Fig. 2(a), the light wave emitted by the LED light source changes into a parallel light wave through the lens. Parallel light passes through the calibration grating and projects the pattern of the calibrated grating onto the image sensor. The image sensor sends the collected pixel data of the calibrated grating pattern to the circuit for processing, and outputs the current displacement value of the angle image sensor as-processed by the angular displacement measurement algorithm. To reduce the optical path volume, we placed the calibration grating snugly against (less than 0.2 mm away) the image sensor.

The linear image sensor is capable only of gathering one-dimensional image information. We designed a calibration grating with single-loop absolute encoding; the calibration grating pattern is shown in Fig. 2(b). The circle of the calibration grating contains 2^8 lines. The Image Detection Area (IDA) of the linear image sensor acquisition area must contain at least eight lines. The wide marking line in the IDA represents "1" and the narrow marking line represents "0". We used M-sequence pseudo-random codes for

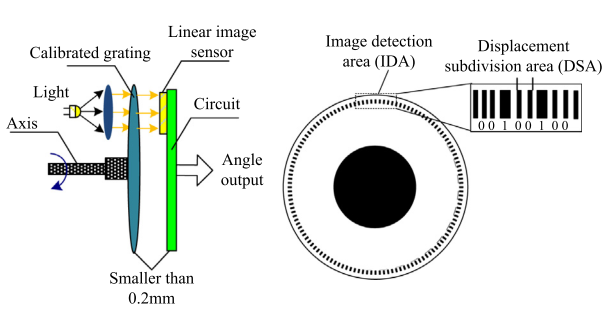

Fig. 2. Image angular displacement measurement principle: (a) Measured optical path; (b) Calibration grating.

encoding, that is, each encoding value was calculated from the XOR between the before eight coded values. We set the i code value to be m_i (i = 9, 10, ..., 255) so that m_i can be calculated as follows:

$$m_i = m_{i-8} \oplus m_{i-3} \oplus m_{i-2} \oplus m_{i-1} \tag{1}$$

where "$\oplus$" marks an XOR operation. We set the initial value $\{m_1, m_2, m_3, \ldots, m_7, m_8\} = \{0,0,0,\ldots,0,1\}$, in addition $m_0 = 0$, to obtain a total of 2^8 coding values via Formula (1). These coded values are characterized by equal equidistant equal radius positions on the circular grating which forms an 8-bit calibration grating. The image sensor determines the current coding value by identifying the width of the IDA inner lines. In Fig. 2(b), for example, the encoding value in the IDA is "0010 0100".

3. High-resolution displacement measurement algorithm

3.1. Displacement algorithm

The area between the two lines in the middle of the IDA is the Displacement Subdivision Area (DSA). In this study, we subdivided the DSA to further improve the angular displacement measurement resolution. The DSA subdivision displacement calculation algorithm is an important aspect of measurement accuracy; a schematic diagram of the process is shown in Fig. 3.

We set a threshold to screen the pixel values of the two markers in the DSA, and only retained pixel values with gray values above the threshold. N pixel values remain after the screening, p_i is the gray value of the i pixel after screening, and the center position of the marking line in A and B can be calculated by the following centroid algorithm:

$$g = \frac{\sum_{i \in N} i \cdot p_i}{\sum_{i \in P} p_i} \tag{2}$$

According to the small angle approximation, the angle value θ in Fig. 3 can be calculated as follows:

$$\theta = \eta \cdot \frac{g_o - g_A}{g_B - g_A} \tag{3}$$

where η is the quantization value for displacement calculation, we set $\eta = 2^n$; g_A, g_B are the centroid of A and B points, respectively, and g_o is the preset location of the center of the collected image.

3.2. Pixel interpolation algorithm

When the image sensor uses relatively few pixels, there may not be enough pixels in the range of the mark line. This pixel insufficiency leads to incorrect angular displacement calculations. The gray value of a typical mark line in a typical DSA is shown in Fig. 4 (a). At certain points in the grating rotation, the gray value of the pixel at the end of the marking line falls below the threshold value and disappears. At this time, the center of mass calculated according to Formula (2) is offset, which produces errors in the angular

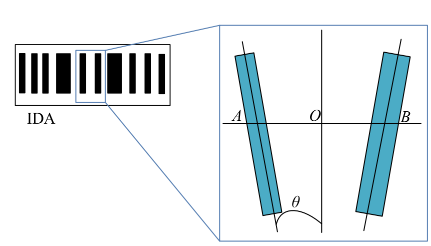

Fig. 3. Schematic diagram of DSA subdivision.

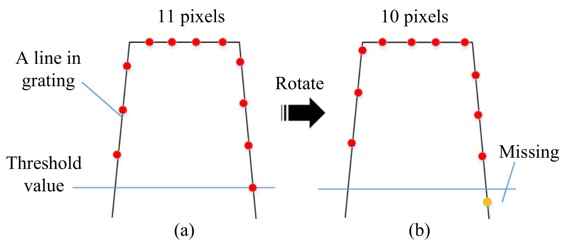

Fig. 4. Image acquisition with insufficient number of pixels.

displacement data rendering the measurements altogether inaccurate (Fig. 4(b)). However, when the number of pixels in the scale range is sufficiently large, the results of Formula (2) are protected.

We propose an interpolation algorithm which inserts the estimated gray value between pixels in the range of markers to improve the efficacy and accuracy of Formulas (2) and (3). After a certain acquired image is filtered by a given threshold, the number of pixels in the range of the mark line is N and the p_i is the gray value of the i pixel. After interpolation, the pixel gray value is h_x; x is the pixel position after interpolation. The gray value $h_{x=2i}$ of the even position can be expressed as follows:

$$h_{2i} = p_i,\ (i = 0, 1, \ldots, N-1) \tag{4}$$

A linear function can be used to estimate the value of h_{2i+1} for the inserted pixel gray value h_{2i+1}:

$$h_{2i+3} = a \cdot (2i+3) + b,\ (i = 0, 1, \ldots, N-2) \tag{5}$$

where a and b are the coefficients to be determined for the linear function. Known pixel values h_{2i} and h_{2i+2} corresponding to each interpolated pixel h_{2i+3} can be used to determine the corresponding coefficients.

$$a = \frac{h_{2i+2} - h_{2i}}{(2i+2) - 2i},\ i = 0, 1, \ldots, N-2 \tag{6}$$

$$b = h_{2i+2} - a \cdot (2i+2),\ i = 0, 1, \ldots, N-2 \tag{7}$$

After determining coefficients a and b, Formula (5) can be used to calculate interpolation h_{2i+3}. After interpolation, the N pixels in the original marking range are changed to $2N-1$ pixel values. The center position of the marking line in A and B can be calculated by Formula (8).

$$g' = \frac{\sum_{x=0}^{2N-1} x \cdot h_x}{\sum_{x=0}^{2N-1} h_x} \tag{8}$$

Formula (8) can then be used to calculate the centroid of the $2N-1$ pixel value and obtain an accurate angular displacement measurement. The new angular displacement measurement arithmetic is show as follow:

$$\theta' = 2^n \cdot \frac{g'_O - g'_A}{g'_B - g'_A} \tag{9}$$

Where, 2^n express 2^n-fold subdivision.

4. Simulations

We used the following Gauss function to simulate gray values of markings to test the proposed interpolation algorithm:

$$y = 50 \cdot e^{\left[\frac{-(x-a_1)^2}{2a_2^2}\right]} \tag{10}$$

We first set the central position of the Gauss function in Formula (10) to $a_1 = 25$ and $a_2 = 4$. The pixel sampling interval of the linear image sensor is 1 and the threshold value is 10. Under normal circumstances, the pixel position collected by the image sensor is as marked by red dots in Fig. 5(a), where the centroid of the red pixel is 25.

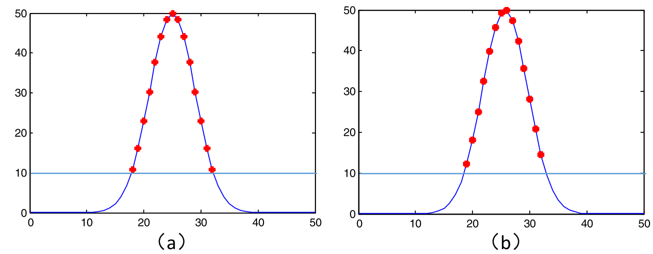

Fig. 5. Gray value curve of simulation.

We changed the center position of the Gaussian function to $a_1 = 25.8$ to obtain the pixel position captured by the image sensor as shown in Fig. 5(b), where the centroid of the red pixel is 25.63 – this value deviates severely from the preset center point $a_1 = 25.8$. The number of pixels in the scale range of the image sensor is small in the case of Fig. 5(b).

We next interpolated the central position of the Gaussian function $a_1 = 25.8$. The interpolation is marked with blue pixels in Fig. 6 and corresponding data is provided in Table 1. The interpolated pixels were used to calculate the center of mass of 25.82, which is relatively near the preset central point $a_1 = 25.8$. In other words, the proposed interpolation calculation enhances measurement accuracy.

5. Experiments

We also used an image angular displacement measurement device to carry out experiments to test the proposed algorithm. The experimental setup is shown in Fig. 7.

In our setup, the linear CCD has a resolution of 1×320 pixels and a pixel interval of 12.7 μm. The diameter of the calibrated grating is 38 mm and there are 256 lines in the circle.

5.1. Image acquisition experiment

We set $\eta = 2^{15}$ in Formula (3), there are $2^8 = 256$ lines in the circumference of the calibrated grating, which produces angular displacement measurement resolution of $360°/2^{23}$. We carefully turned the spindle and re-calculated Formula (3) to find that the output value was incorrect in certain positions. We continuously collected the center of mass of one of the markers, as shown in Fig. 8, as we rotated the spindle at a slow and constant speed. The centroid calculation (Fig. 8) spikes at position No.13 to produce an incorrect output angle.

We performed image acquisitions before and after another output error, as shown in Fig. 9, to further assess the performance of

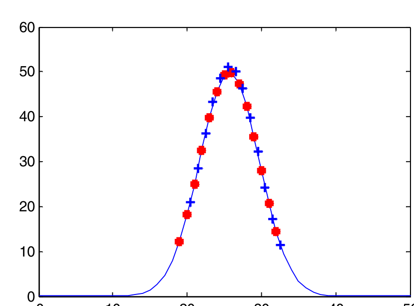

Fig. 6. Pixel gray curve after interpolation.

Table 1
Simulation data.

Position	**19**	**20**	**21**	**22**	**23**	**24**	**25**	**26**	**27**	**28**	**29**	**30**	**31**	**32**
Values	12.3	18.1	25.1	32.6	39.8	45.7	49.2	49.9	47.4	42.4	35.6	28.1	20.8	14.5
Position		**20.5**	**21.5**	**22.5**	**23.5**	**24.5**	**25.5**	**26.5**	**27.5**	**28.5**	**29.5**	**30.5**	**31.5**	**32.5**
Values		21.0	28.5	36.4	43.4	48.6	51.0	50.2	46.2	39.9	32.2	24.3	17.1	11.3

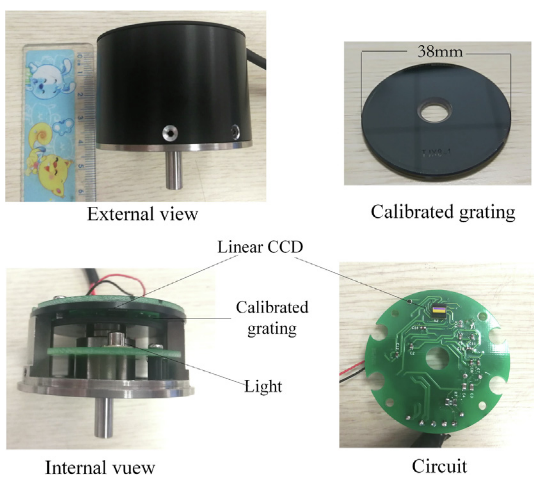

Fig. 7. Experimental device for angular displacement measurement.

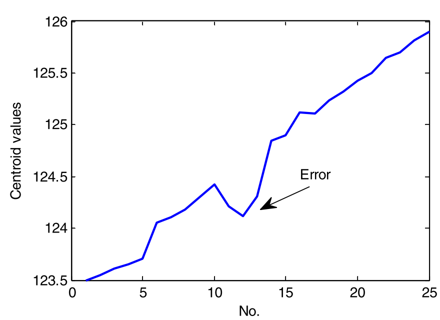

Fig. 8. Centroid data curve.

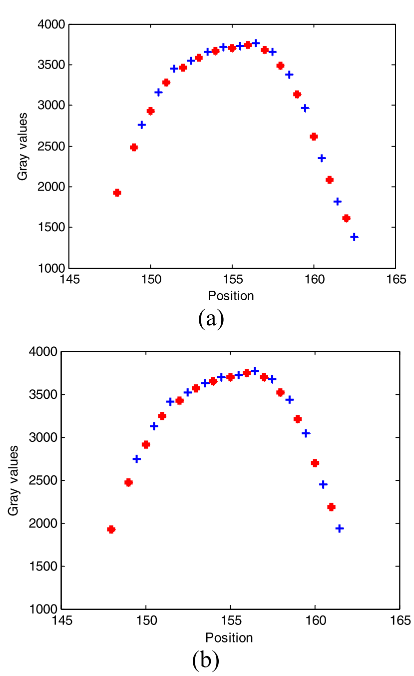

Fig. 9. Gray values collected. (a) before error occurs, (b) after error occurs.

Table 2
Error values.

Angles(°)	Errors(″)	Angles(°)	Errors(″)
0	0	195	15
15	−1	210	10
30	−7	225	15
45	−15	240	20
60	−23	255	24
75	−14	270	25
90	−17	285	21
105	3	300	15
120	2	315	10
135	3	330	11
150	10	345	7
165	11	360	0
180	12		

the proposed algorithm. Fig. 9(a) shows the gray value curve pre-error and Fig. 9(b) shows the gray value curve of the error. The red dots in Fig. 9(a) are the pixel values captured by the image sensor when the threshold is 1500. The centroid position of the red dots is 154.86 as-calculated by the centroid algorithm; the centroid position of the red dots in Fig. 9(b) is 154.64. The difference in centroid position before and after the output error is 0.22 as per the original image sensor data.

The pixels inserted after the interpolation algorithm are marked with blue dots in Fig. 9. At this point, the interpolated center of mass in Fig. 9(a) is 155.14, the interpolated center of mass in Fig. 9(b) is 154.95, and the interpolated value is 0.19; the output data is correct. We again rotated the main shaft of the experimental device carefully and observed all data output normally under the proposed algorithm. We found that the proposed algorithm reliably achieves $360°/2^{23}$ angular displacement measurement resolution.

5.2. Accuracy test experiment

We applied the proposed algorithm to the experimental device in Fig. 7 to determine the resulting angular displacement measurement accuracy. We also tested the measurement error by using an angle reference. The experimental device and the angle reference were coaxially coupled throughout the test. The angle reference and the experimental device outputs were collected every 15° and the error value obtained by calculating the difference between

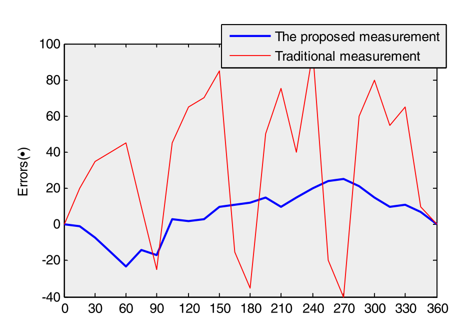

Fig. 10. Error contrast results.

them. A total of 25 error points were recorded in the circle as shown in Table 2.

The mean square error of the error values in Table 2 is 12.93″. We compared the test data with a traditional moiré fringe angle measurement device to further assess its performance. The resulting contrast curves are shown in Fig. 10.

The red curve in Fig. 10 is the error values of the traditional moiré fringe measurement method, the mean square deviation of which is 39.61″. The blue curve is the proposed measurement error curve, which has a mean square deviation of 12.93″. The proposed angle measurement method is far superior to the traditional measurement method in terms of accuracy.

6. Conclusion

A high-resolution image angular displacement measurement algorithm based on pixel interpolation was proposed in this paper. We collected the gray value of a grating marking pattern by image sensor and interpolated the positions between adjacent pixels to significantly improves the resolution of the traditional measurement device. This technique can effectively enhance the resolution of the traditional image sensor for enhanced displacement measurement accuracy.

We analyzed the influence of insufficient pixel quantity in the grating marking range on the angular displacement measurement according to the optical path of small images in the device. We established a high-resolution angular displacement measuring algorithm based on pixel interpolation accordingly. Simulations demonstrated that the proposed algorithm significantly enhances calculation accuracy. When applied to an experimental device, the algorithm produced measurement resolution of $360°/2^{23}$ and 12.93″ mean square deviation of measurement error. To this effect, the proposed algorithm may provide a theoretical basis for further research on small angle displacement measurement technology.

Funding

This project is supported by National Natural Science Foundation of China (Grant No. 51605465), Science and Technology Development Programme of Jilin Province (Grant No. 20180520184JH).

Declaration of Competing Interest

The authors declare that they have no known competing financial interests or personal relationships that could have appeared to influence the work reported in this paper.

References

[1] K. Hane, T. Endo, Y. Ito, M. Sasaki, A compact optical encoder with micro machined photodetector, Opt. A: Pure Appl. Opt. 191–5 (2001).
[2] K. Hane, T. Endo, M. Ishimori, M. Sasaki, Integration of grating-image-type encoder using Si micromachining, Sens., Actuators A 97 (2002) 139–146.
[3] F. Liu, W. Wang, L. Wang, P. Feng, Error analyses and calibration methods with accelerometers for optical angle encoders in rotational inertial navigation systems, Appl. Opt. 52 (2013) 7724–7731.
[4] Z. Hongbo, W. Qiuhua, W. Shujie, Y. Hai, L. Lihui, Installation error control of dynamic measurement for small photoelectric encoder, Opt. Precis. Eng. 24 (2016) 1655–1660 (in Chinese).
[5] H. Yu, W.Q. Hua, X.R. Lu, C.H. Zhao, L.H. Liang, Calibration of dynamic precision for measurement platform of photoelectric encoder, Opt. Precis. Eng. 24 (2016) 2699–2704 (in Chinese).
[6] K. Patorsky, M. Kujawinska, Handbook of the Moiré Fringe Technique, Elsevier, Amsterdam, Holland, 1993.
[7] Q.H. Wan, Y. Sun, S.J. Wang, R.H. She, X.R. Lu, L.H. Liang, Design for spaceborne absolute photoelectric encoder of dual numerical system, Opt. Precis. Eng. 17 (2009) 52–57 (in Chinese).
[8] F. Deng, J. Chen, Y.Y. Wang, K. Gong, Measurement and calibration method for an optical encoder based on adaptive differential evolution-Fourier neural networks, Meas. Sci. Technol. 24 (2013) 055008.
[9] A. Lutenberg, F. Perez-Quintián, Optical encoder based on a nondiffractive beam III, Appl. Opt. 48 (2009) 5015–5024.
[10] W. Luo, Y. Zhang, A. Feizi, Z. Gorocs, A. Ozcan, Pixel super-resolution using wavelength scanning, Light Sci. Appl. 5 (2016) e16060.
[11] J. Qin, R.M. Silver, B.M. Barnes, H. Zhou, R.G. Dixson, M. Henn, Deep subwavelength nanometric image reconstruction using Fourier domain optical normalization, Light Sci. Appl. 5 (2016) e16038.
[12] S. Witte, V.T. Tenner, D.W. Noom, K.S. Eikema, Lensless diffractive imaging with ultra-broadband table-top sources: from infrared to extreme-ultraviolet wavelengths, Light Sci. Appl. 3 (2014) e163.
[13] V.J. Cadarso, S. Chosson, K. Sidler, R.D. Hersch, J. Brugger, High-resolution 1D moire's as counterfeit security features, Light Sci. Appl. 2 (2013) e86.
[14] A.C. Sobieranski, F. Inci, H.C. Tekin, M. Yuksekkaya, E. Comunello, D. Cobra, A. von Wangenheim, U. Demirci, Portable lensless wide-field microscopy imaging platform based on digital inline holography and multi-frame pixel super-resolution, Light Sci. Appl. 5 (2015) e346.
[15] V. Bianco, P. Memmolo, M. Paturzo, A. Finizio, B. Javidi, P. Ferraro, Quasi noise-free digital holography, Light Sci. Appl. 5 (2016) e16142.
[16] D.B. Leviton, B.J. Frey, Ultra-high resolution, absolute position sensors for cry static applications, Proc. SPIE 4850 (2003) 776–787.
[17] D.B. Leviton, M.S. Garza, Recent advances and applications for NASA's new, ultra-high sensitivity, absolute, optical pattern recognition encoders, Proc. SPIE 4091 (4091) (2003) 375–384.
[18] Y. Sugiyam, Y. Matsu, H. Toyod, N. Mukozaka, A. Ihori, T. Abe, M. Takabe, S. Mizuno, A 3.2 kHz 14-bit optical absolute rotary encoder with a CMOS profile sensor, IEEE Sens. J. 8 (2008) 1430–1436.
[19] M. Tresanchez, T. Pallejà, M. Teixidó, J. Palacín, Using the image acquisition capabilities of the optical mouse sensor to build an absolute rotary encoder, Sens. Actuators A 157 (2010) 161–167.
[20] J.A. Kim, J.W. Kim, C.S. Kang, J. Jin, T.B. Eom, Absolute angle measurement using a phase-encoded binary graduated disk, Measurement 80 (2016) 288–293.
[21] Y.N. Wang, B. Yaun, X.X. Ni, Subdivision technique of absolute angular encoder using array detector, Zhejiang Univ. (Engineering Science) 45 (2011) 370–374 (in Chinese).
[22] L.L. Qi, Angle-measurement technology of an optical pattern rotary encoder and its hardware implementation, Acta Opt. Sin. 33 (2013) 0412001, in Chinese.
[23] H. Yu, Q.H. Wan, X.R. Lu, Y.C. Du, S.W. Yang, Small-size, high-resolution angular displacement measurement technology based on imaging detector, Appl. Opt. 56 (2017) 755–760.
[24] H. Yu, Q.H. Wan, X.R. Lu, C.H. Zhao, Y.C. Du, A robust sub-pixel subdivision algorithm for image-type angular displacement measurement, Opt. Laser. Eng. 100 (2018) 234–238.